K

LEVEL

DNA 5148T

MEASURING AND INTERPRETING ELF SIGNALS DURING A PCA

Aspects of an Experimental Design

E. C. Field, Jr.

R. N. DeWitt

Pacific-Sierra Research Corporation
1456 Cloverfield Boulevard
Santa Monica, California 90404

DTIC
ELECTE
OCT 9 1980
S
C

1 December 1979

Topical Report for Period 1 December 1978—1 December 1979

CONTRACT No. DNA 001-79-C-0015

APPROVED FOR PUBLIC RELEASE;
DISTRIBUTION UNLIMITED.

Prepared for

Director

DEFENSE NUCLEAR AGENCY

Washington, D. C. 20305

Destroy this report when it is no longer
needed. Do not return to sender.

REPORT DOCUMENTATION PAGE	READ INSTRUCTIONS BEFORE COMPLETING FORM

1 REPORT NUMBER	2 GOVT ACCESSION NO.	3 RECIPIENT'S CATALOG NUMBER
DNA 5148T	AD-A090 121	

4 TITLE (and Subtitle)

MEASURING AND INTERPRETING ELF SIGNALS DURING A PCA Aspects of an Experimental Design

5 TYPE OF REPORT & PERIOD COVERED

Topical Report, for Period 1 Dec 78— 1 Dec 79

6 PERFORMING ORG. REPORT NUMBER

PSR Report 932

7 AUTHOR(s)

E. C. Field, Jr.
R. N. DeWitt

8 CONTRACT OR GRANT NUMBER(s)

DNA001-79-C-0015

9 PERFORMING ORGANIZATION NAME AND ADDRESS

Pacific-Sierra Research Corp.
1456 Cloverfield Blvd.
Santa Monica, California 90404

10 PROGRAM ELEMENT PROJECT, TASK AREA & WORK UNIT NUMBERS

Subtask S99QAXHB042-21

11 CONTROLLING OFFICE NAME AND ADDRESS

Director
Defense Nuclear Agency
Washington, D.C. 20305

12 REPORT DATE

1 December 1979

13 NUMBER OF PAGES

52

14 MONITORING AGENCY NAME & ADDRESS(if different from Controlling Office)

15 SECURITY CLASS (of this report)

UNCLASSIFIED

15a DECLASSIFICATION DOWNGRADING SCHEDULE

16 DISTRIBUTION STATEMENT (of this Report)

Approved for public release; distribution unlimited.

17 DISTRIBUTION STATEMENT (of the abstract entered in Block 20, if different from Report)

18 SUPPLEMENTARY NOTES

19 KEY WORDS (Continue on reverse side if necessary and identify by block number)

Experimental design	Rocket measurements
Nuclear effects	Signal strength measurement
Polar cap absorption	Transpolar ELF propagation
Propagation codes	

20 ABSTRACT (Continue on reverse side if necessary and identify by block number)

Investigates the design of a transpolar extremely-low-frequency (ELF) experiment that would validate Defense Nuclear Agency propagation codes for ELF system performance in nuclear environments. To be conducted during the next solar maximum, when polar cap absorption events (PCAs) might approximate a nuclear environment, the ideal experiment would simultaneously measure both propagation and ionospheric structure. Propagation measurements would be taken at receivers located such that the direct propagation path did not approach the polar cap boundary; the ELF values would then be compared with computer

20. ABSTRACT (Continued)

code outputs. A moderate PCA might cause a 3 to 4 dB reduction in a transpolar
ELF signal; a strong event, an 8 or 9 dB reduction. At least 2 hours would be
required to resolve amplitude changes in the signal; noise processing to excise
large pulses would be essential. Measurements of ionospheric changes would be
taken with rocket-borne instruments, entered into computer calculations using
the DNA codes, then compared with the propagation measurements. Rocket data
should be gathered at 50 km or below; data from previous PCAs obtained only
at 60 km or above yield unacceptable uncertainties in calculated field strengths.

Accession For

NTIS GRA&I
DTIC TAB
Unannounced
Justification

By
Distribution/
Availability Codes
         Avail and/or
Dist   Special

A

SUMMARY AND CONCLUSIONS

This report investigates the design of a transpolar extremely-low-frequency (ELF) experiment that would validate Defense Nuclear Agency codes for predicting ELF propagation in nuclear environments. Such an experiment would be conducted during a maximum in the solar cycle, when disturbances in the polar ionosphere--polar cap absorption events, or PCAs--caused by solar disruptions would resemble distortions in the earth-ionosphere waveguide caused by radiation from a high-altitude nuclear burst.

The most effective experiment would simultaneously measure both propagation and ionospheric structure. Propagation measurements would be accomplished with one or more receivers placed (e.g., in Norway) so that an ELF signal transmitted from the Wisconsin Test Facility (WTF) traversed at least a few megameters of the polar cap (but without obliquely intersecting the cap boundary, to avoid transverse edge effects that would complicate interpretation of the measurements). Changes in the WTF signal measured during a PCA would then be compared with field-strength values calculated from the ELF predictive codes--thereby checking the codes. Data necessary for calculating refractive-index height profiles (the basic inputs to the codes)--height profiles of electron density, ion density, or positive and negative conductivity in the lower ionosphere--would be obtained using rocket-borne instruments.

The propagation measurements would have to determine signal changes whose uncertainty was much smaller than the expected PCA-induced reductions (3 to 4 dB from a moderate PCA, 8 or 9 dB from a strong PCA); otherwise, experimental errors would mask the PCA's effect. Resolving amplitude changes from a large PCA would require at least two hours of integration, since a transpolar WTF signal would be very weak. Noise processing to excise large pulses would be essential.

To minimize uncertainties in ELF signal strength calculated from the predictive codes, electron density data should be obtained at

-1-

altitudes of 50 km or below, where electrons strongly affect ELF propagation; rocket measurements of ionospheric structure made during previous PCAs obtained data only for altitudes of 60 km or above, yielding unacceptable uncertainties. To obtain data at lower altitudes would require sensing a few tens of electrons per cubic centimeter in a collision-dominated region.

Uncertainties in interpreting the results (that is, in comparing measured with calculated changes in field strength) related to the excitation factor at the ELF receiver could be avoided by (1) locating the receiver so that there was no doubt whether it was inside or outside the irradiated cap, or (2) sounding the ionosphere at the receiver site.

PREFACE

This report documents contingency planning--requested by the
Defense Nuclear Agency--for a transpolar extremely-low-frequency
(ELF) propagation experiment to be performed during the forthcoming
maximum in the solar cycle. The experiment would verify theoretical
predictive codes under disturbed ionospheric conditions. Even though
budgetary constraints will probably prohibit the experiment, the
present analysis should assist the designers of future experiments
that require coordinated measurements of ELF signal strength and
ionospheric structure.

TABLE OF CONTENTS

LIST OF ILLUSTRATIONS

LIST OF TABLES

SECTION 1

INTRODUCTION

Propagation codes developed by the Defense Nuclear Agency (DNA) to predict extremely-low-frequency (ELF) system performance in nuclear environments have not been fully verified experimentally. Pacific-Sierra Research Corporation (PSR) was requested by DNA to investigate certain aspects of the design of a transpolar propagation experiment to validate these codes. Such an experiment would be performed during a maximum in the solar cycle, when polar cap absorption events (PCAs) would be expected to simulate salient aspects of nuclear environments. This report summarizes the results of our investigation and establishes minimum tolerances for a definitive verification of ELF propagation codes.

Radiation from high-altitude nuclear bursts ionizes the atmosphere below the ambient, ionospheric D- and E-layers--a distortion of the earth-ionosphere waveguide that may affect military long-wave communication systems. Computer codes predict that a link with at least several megameters of propagation path exposed to such an environment can suffer significant signal loss. That conclusion has been substantiated experimentally for low- and very-low-frequency (LF/VLF) links, for which data are available from (1) the Fish Bowl high-altitude nuclear test series, (2) a laboratory model of the earth-ionosphere waveguide [Field et al., 1972], and (3) propagation experiments under naturally disturbed conditions [Westerlund et al., 1969].

ELF communications (45 to 100 Hz) are much newer than LF/VLF communications, operational for decades. The only existing ELF transmitter is the low-power Wisconsin Test Facility (WTF) constructed quite recently. The data on ELF propagation are thus much less comprehensive than those on LF/VLF. Indeed, data on disturbed conditions are limited to a few fortuitous measurements of natural ELF signals (atmospheric noise) during high-altitude tests and natural ionospheric disturbances.

Field [1978] found the sparse data generally consistent with computer predictions of degraded propagation for severe and widespread disturbances. Nonetheless, no experiment has yet monitored a signal from a controlled ELF source during a strong ionospheric disturbance. The probable increase in the number and magnitude of PCAs during the approaching maximum in the 11 year solar cycle should afford such an opportunity.

A PCA approximates certain features of a nuclear environment, since solar conditions cause energetic protons to penetrate and ionize the polar ionosphere to altitudes as low as 40 km. The most effective experiment would simultaneously measure propagation and ionospheric structure. Propagation measurements would quantify changes in the WTF signal during a PCA, thus providing values to compare with computer code outputs. Such measurements would be accomplished with one or more receivers placed so the signal traverses at least a few megameters of the polar cap. Values quantifying changes in the ionospheric structure would be entered into the computer programs for calculating field-strength changes to compare with measured values--thereby checking the codes. Such measurements could be accomplished with, for example, rocket-borne instruments.

Our analysis shows that a moderate PCA might cause a 3 to 4 dB reduction in a transpolar ELF signal, whereas a strong event might cause an 8 or 9 dB reduction. The propagation measurements must determine signal changes with an uncertainty much smaller than the expected PCA-induced reductions; otherwise, experimental errors will mask the effect to be studied. Similarly, ionospheric measurements used as code inputs must be accurate enough for meaningful comparison of calculated and measured signal changes.

Sections 2 and 3 consider the measurement of ionospheric structure. Section 2 examines data from rocket samplings of vertical ionospheric structure during previous PCAs, identifying inadequacies that must be corrected for future experiments. Section 3 examines the propagation effects of lateral ionospheric structure in the polar cap, quantifies computational uncertainties caused by such structure, and compares the uncertainties with the minimum tolerances required for code verification.

Section 4 addresses the problem of weak transpolar WTF signal, which must be integrated for an accurate estimate of received signal. Too short an integration time causes unacceptable uncertainty in amplitude. Conversely, too long an integration time may create uncertainties due to substantial changes in the incident flux and ionospheric ionization during measurement. Criteria are established for the best compromise on integration time. The benefits of nonlinear suppression of atmospheric noise at the receiver are also quantified.

SECTION 2

ROCKET MEASUREMENTS OF IONOSPHERIC STRUCTURE FOR USE AS INPUTS TO ELF PROPAGATION CALCULATIONS

Rocket-borne instruments measure the height profiles of electron density, ion density, or positive and negative conductivity in the lower ionosphere. Such data are needed to calculate refractive-index height profiles, which are the basic inputs to ELF predictive codes. Thus rocket data permit a direct comparison of measured and calculated ELF field strengths for ionospheric conditions at the time of propagation. Here we summarize the formulas for converting measured ionospheric parameters to refractive index profiles, identify inaccuracies, and establish criteria for precision of measurement.

FORMULAS FOR REFRACTIVE INDEX

Rocket data can most easily be converted to the refractive index when the positive and negative conductivities σ_+ and σ_- are measured directly. In this case, the refractive index n is calculated from

$$n^2 = 1 - \frac{i}{\omega \epsilon_0} (\sigma_+ + \sigma_-) . \tag{1}$$

Since $\epsilon_0 = 8.85 \times 10^{-12}$ and the angular frequency ω is known exactly, the accuracy of the refractive index computed from Eq. (1) is equivalent to that of the measured data for the conductivities. However, Eq. (1) is valid only if σ_+ and σ_- denote the cumulative conductivities of all positive and negative species, respectively. It could be grossly in error at certain altitudes if, for example, the instrument used to measure σ_- could fully sense the conductivity of ions but not electrons.

Unfortunately, the refractive index is less accurate when based on electron density N_e, positive ion density N_α^+, and negative ion

-10-

density N_β^- instead of conductivity.[*] In that situation, the ELF refractive index at heights below about 75 km is calculated from

$$n^2 \approx 1 - i \frac{q^2}{\omega \epsilon_0} \left(\frac{N_e}{M_e \nu_e} + \sum_\alpha \frac{N_\alpha^+}{M_\alpha \nu_\alpha} + \sum_\beta \frac{N_\beta^-}{M_\beta \nu_\beta} \right) , \qquad (2)$$

where q is the electron charge, M_e is the electron mass, ν_e is the electron collision frequency, M_α is the mass of the αth positive ion, ν_α the collision frequency of the αth positive ion, and so forth.

Comparing Eq. (2) with Eq. (1), we find that

$$\sigma_+ = \sum_\alpha \frac{N_\alpha^+ q^2}{M_\alpha \nu_\alpha} \qquad (3a)$$

and

$$\sigma_- = \frac{N_e q^2}{M_e \nu_e} + \sum_\beta \frac{N_\beta^- q^2}{M_\beta \nu_\beta} . \qquad (3b)$$

Thus the refractive index--or, equivalently, the conductivities--must be synthesized by summing over *all* charged species sufficiently populous to make a significant contribution. The terms in the sums are not governed solely by the particle densities, but instead depend on the combination $N/M\nu$ for each species. That dependence causes no serious loss of accuracy when the conductivity (or refractive index) is dominated by electrons, because the electron mass is exact and ν_e is believed to be known accurately. However, the ion collision frequencies are uncertain by a factor of 2, and masses of important ion species are often imprecise. At lower altitudes where ions dominate the refractive index, therefore, *the combination $N/M\nu$ is known no*

---

[*] To accommodate the large number of ionic species, we use the subscripts α and β to denote the "αth" and "βth" positive and negative species.

better than to within a factor of 2 or 3 even if the ion density N is precise. In principle, that uncertainty can be avoided by directly measuring conductivities at ion-dominated altitudes, because, as Eq. (3) shows, such measurements directly determine the sum of N/Mν over all important species.

In practice, the full sums in Eq. (2) are seldom used in engineering calculations. Ionic species are classified as simply "positive" or "negative" ions, each type having properties determined by averaging over the species actually present. Further, it is usually assumed that such generic ions have equal masses M_i and collision frequencies ν_i. Equation (2) then takes the simplified form

$$n^2 \approx 1 - i \frac{q^2}{\omega\varepsilon_0} \left(\frac{N_e}{M_e\nu_e} + \frac{N^+ + N^-}{M_i\nu_i} \right) , \qquad (4)$$

where N^+ and N^- are the densities of the "average" positive and negative ions, respectively. The values of M_i and ν_i at a given altitude are uncertain. We use an atomic weight of 32 here for M_i, but--depending on altitude--values as low as 19 or as high as 50 or 60 are possible. Similarly, ν_i could be anywhere from a tenth to a fortieth of ν_e; we follow current convention in assuming $\nu_i = \nu_e/20$.

We use Eq. (1) to compute the refractive index from blunt-probe conductivity data. Inserting the value for ε_0 and assuming a frequency of 75 Hz, Eq. (1) becomes

$$n^2 - 1 = -2.4i \times 10^8 (\sigma_+ + \sigma_-) , \qquad (5)$$

where σ_+ and σ_- are in mhos per meter.

We use Eq. (4) to compute the refractive index from data on electron and ion density. Since $N^- \approx N^+$ whenever ions contribute significantly to the refractive index, we can rewrite Eq. (4) as

$$n^2 - 1 = -i \frac{q^2}{\omega\varepsilon_0 M_e\nu_e} \left(N_e + \frac{2M_e\nu_e}{M_i\nu_i} N^+ \right) . \qquad (6)$$

Substituting numerical values and assuming $M_i = 32$ and $\nu_i = \nu_e/20$, Eq. (6) becomes

$$n^2 - 1 \approx - \frac{6.75i}{\nu_e} \left(N_e + \frac{N^+}{1500} \right) , \qquad (7)$$

where N_e and N^+ are in units of $(meters)^{-3}$ and ν_e is taken from Knapp and Schwartz [1975, Fig. 5-1].

We can determine n^2 accurately from density data at high, electron-dominated altitudes because the parameters in the electron contributions to Eq. (7) are well known. Similarly, at low, ion-dominated altitudes, the problem of poorly known ν_i and M_i can be circumvented by measuring ion conductivity directly and using Eq. (5) to determine the refractive index. Potential difficulties arise in the transition region where, although much less numerous than ions and difficult to measure, electrons still make a major contribution to n^2. Unfortunately, that region occurs at altitudes crucial to ELF propagation.

For example, as Eq. (7) demonstrates, the transition from electron to ion dominance occurs at the altitude where

$$N_e \approx \frac{N^+}{1500} . \qquad (8a)$$

More explicitly, we can write

$$N_e \gtrsim \frac{N^+}{1500} \qquad \text{(electrons dominate)} \qquad (8b)$$

and

$$N_e \lesssim \frac{N^+}{1500} \qquad \text{(ions dominate)} . \qquad (8c)$$

Even at altitudes where, say, $N_e \sim 10^{-3} N^+$, therefore, electron density must be measured accurately. As shown below, this requirement implies measurement of a few tens of electrons per cubic centimeter at altitudes of 50 to 60 km during a PCA.

EXAMPLE: *PCA 69*

Using data from the PCA of 2 November 1969, we now consider problems encountered in using rocket measurements of ionospheric structure for ELF propagation calculations. Other PCAs have been stronger or possibly more interesting, but none has been so carefully monitored. A series of rocket measurements using several sensor types are reported in the *Proceedings of COSPAR Symposium on Solar Particle Event of November 1969*, henceforth called *PCA 69*. The papers by Hale et al. and Ulwick, cited below, appear in that report.

Of primary interest are blunt-probe measurements of σ_+ and σ_- given by Hale et al. [1972] and the following measurements given by Ulwick [1972]: Langmuir probe (LP) measurements of N_e and N^+, Z-0 probe measurements of N_e, and Gerdien condenser (GC) measurements of N^+. Here we compute the ELF refractive index using selected samples of those data, thereby stressing inconsistencies among the measurements and altitude gaps where the data are inadequate.

Table 1 lists $|n^2 - 1|$ at various altitudes, calculated from Eq. (5) using the conductivity measurements of Hale et al. [1972]; and from Eq. (7) using the electron and ion density data summarized by Ulwick [1972]. Results are given for sunrise, daytime, and sunset on 3 November 1969--the day after the onset of the event.

For convenience, Figs. 1 through 3 plot the refractive index curves for $|n^2 - 1|$ at various altitudes from Table 1. The lower altitude portions of the curves show ions only, since Ulwick reports no N_e values for those regions (recall that $N^+ + N^- \approx 2N^+$). At sufficiently low altitudes, the "ions only" refractive index should approximate the total index. At higher altitudes, the Ulwick data give the total refractive index, including both electrons and ions, but are dominated by the highly mobile electrons. At altitudes for which Table 1 lists data for both N^+ and N_e, we have prorated the contribution of ions according to Eq. (7), thereby extending the "ions only" curves.

-14-

Table 1. Comparison of refractive-index height profiles at 75 Hz computed from various rocket data; 3 November 1969.

Sunrise

Altitude (km)	Hale et al. (805 LT) σ_+	σ_-	$\lvert n^2 - 1 \rvert$	Ulwick (752 LT) N_e (Z-θ)	N^+ (LP)	$\lvert n^2 - 1 \rvert$
25	6×10^{-12}	6×10^{-12}	2.8×10^{-3}	--	--	--
30	10^{-11}	10^{-11}	4.8×10^{-3}	--	--	--
35	4.5×10^{-11}	4.5×10^{-11}	2.2×10^{-2}	--	--	--
40	3.5×10^{-10}	10^{-9}	0.32	--	7×10^3	6.3×10^{-2}
45	1.2×10^{-9}	1.2×10^{-9}	1.1	--	10^4	0.22
50	2.2×10^{-9}	8×10^{-9}	2.4	--	1.6×10^4	0.72
55	4×10^{-9}	10^{-8}	4.4	--	3.2×10^4	2.1
60	--	--	--	10^3	4×10^4	225
65	--	--	--	4×10^3	4×10^4	1.8×10^3
70	--	--	--	8×10^3	1.2×10^4	6.7×10^3
75	--	--	--	1.1×10^4	1.1×10^4	10^4

Noon

Altitude (km)	Hale et al. (1029 LT) σ_+	σ_-	$\lvert n^2 - 1 \rvert$	Ulwick (1111 LT) N_e (LP)	N^+ (GC)	$\lvert n^2 - 1 \rvert$
25	2×10^{-12}	2×10^{-12}	3.4×10^{-3}	--	--	--
30	1.3×10^{-11}	1.3×10^{-11}	6.2×10^{-3}	--	--	--
35	5×10^{-11}	5×10^{-11}	2.4×10^{-2}	--	--	--
40	2.2×10^{-10}	4×10^{-9}	1.0	--	--	--
45	1.3×10^{-9}	5×10^{-9}	1.5	--	1.1×10^4	0.17
50	2.2×10^{-9}	7×10^{-9}	2.3	--	1.5×10^4	0.68
55	4×10^{-9}	1.5×10^{-8}	4.6	--	10^4	0.68
60	--	--	--	--	10^4	1.5
65	--	--	--	--	8×10^3	1.8
70	--	--	--	1.1×10^4	1.1×10^4	8.2×10^3
75	--	--	--	2×10^4	2×10^4	10^4

Sunset

Altitude (km)	Hale et al. (no data) σ_+	σ_-	$n^2 - 1$	Ulwick (1708 LT) N_e (Z-θ)	N^+ (GC)	$\lvert n^2 - 1 \rvert$
25	--	--	--	--	--	--
30	--	--	--	--	--	--
35	--	--	--	--	--	--
40	--	--	--	--	--	--
45	--	--	--	--	10^4	0.15
50	--	--	--	--	1.5×10^4	0.68
55	--	--	--	--	1.5×10^4	0.97
62.5	--	--	--	3.5×10^2	2×10^4	45
65	--	--	--	9×10^2	1.5×10^4	300
70	--	--	--	3×10^3	1×10^4	2.25×10^3
75	--	--	--	5×10^3	1×10^4	10^4

NOTE: Not all sensors were operating at the three times considered: Hale et al. give no conductivity data for sunset, and Ulwick obtained no Gerdien condenser measurements at sunrise. All measurements reported by Hale et al. were made with a blunt probe, whereas the method (Z-θ, LP, or GC) used to obtain the data given by Ulwick are indicated at the top of each column. LT = local time. Hale et al. give values of conductivity in mhos per meter. Ulwick's measurements are in units of (centimeters)$^{-3}$.
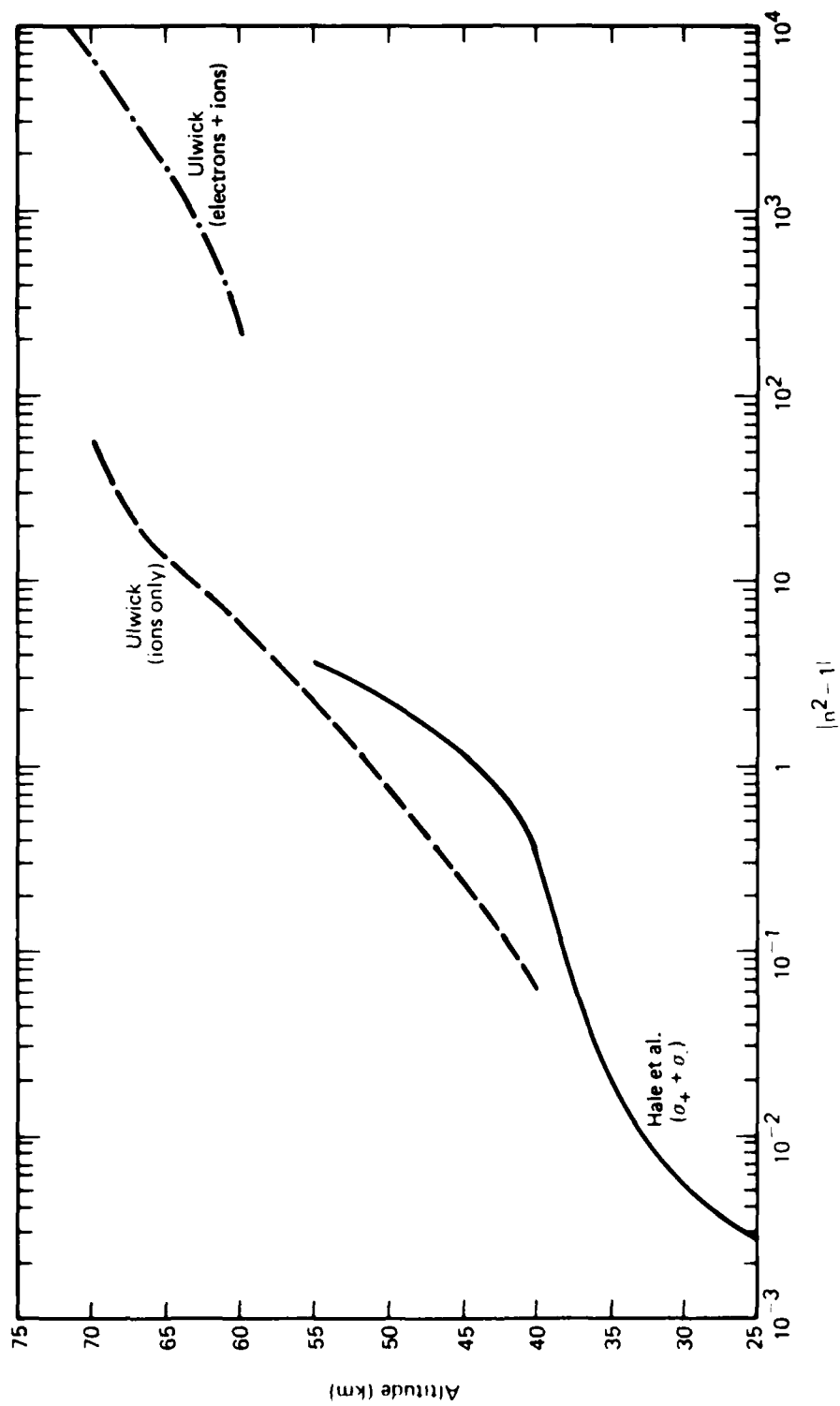
-15-

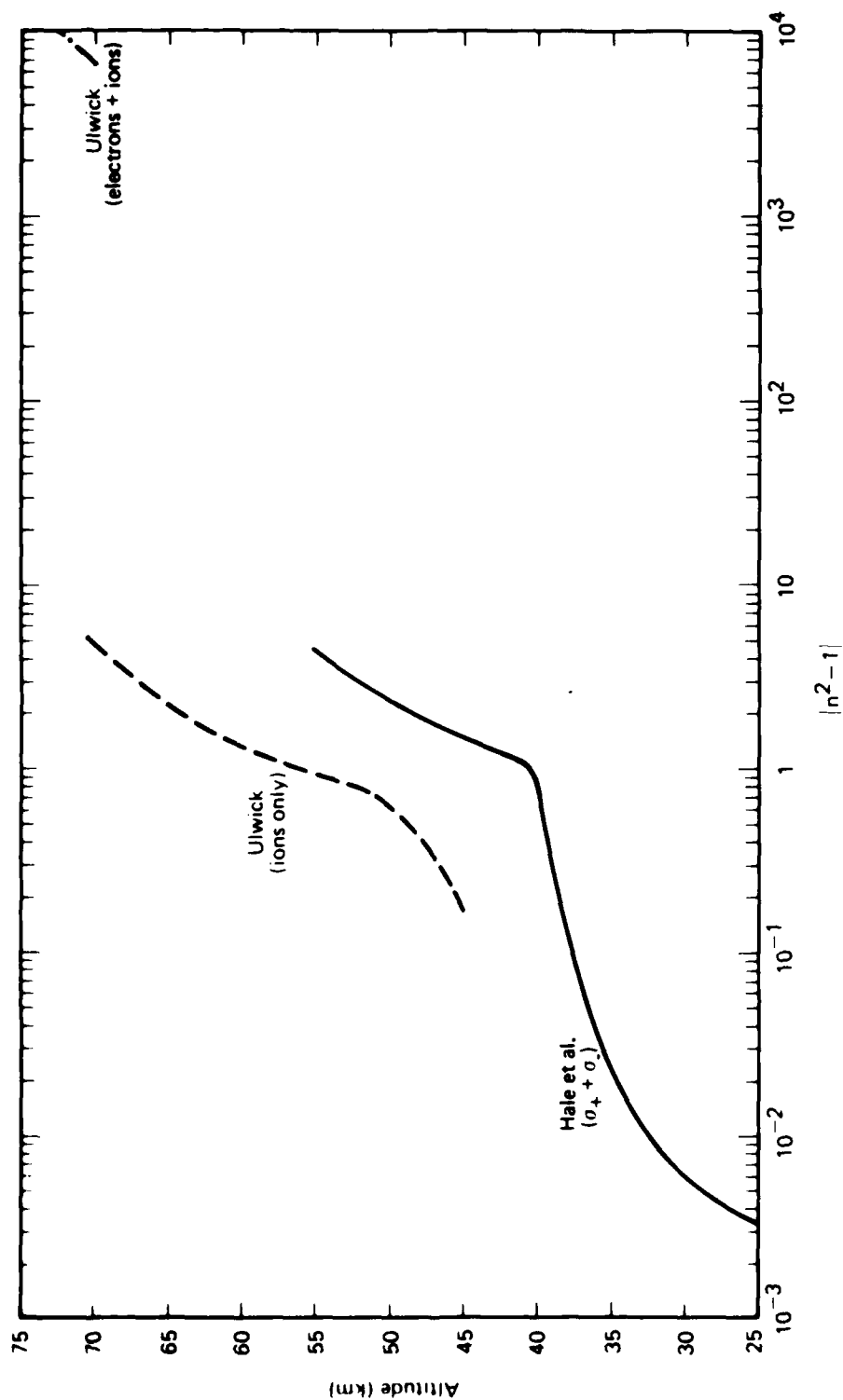Figure 1. Refractive-index height profiles at 75 Hz: sunrise, 3 November 1969.

Figure 2. Refractive-index height profiles at 75 Hz: daytime, 3 November 1969.
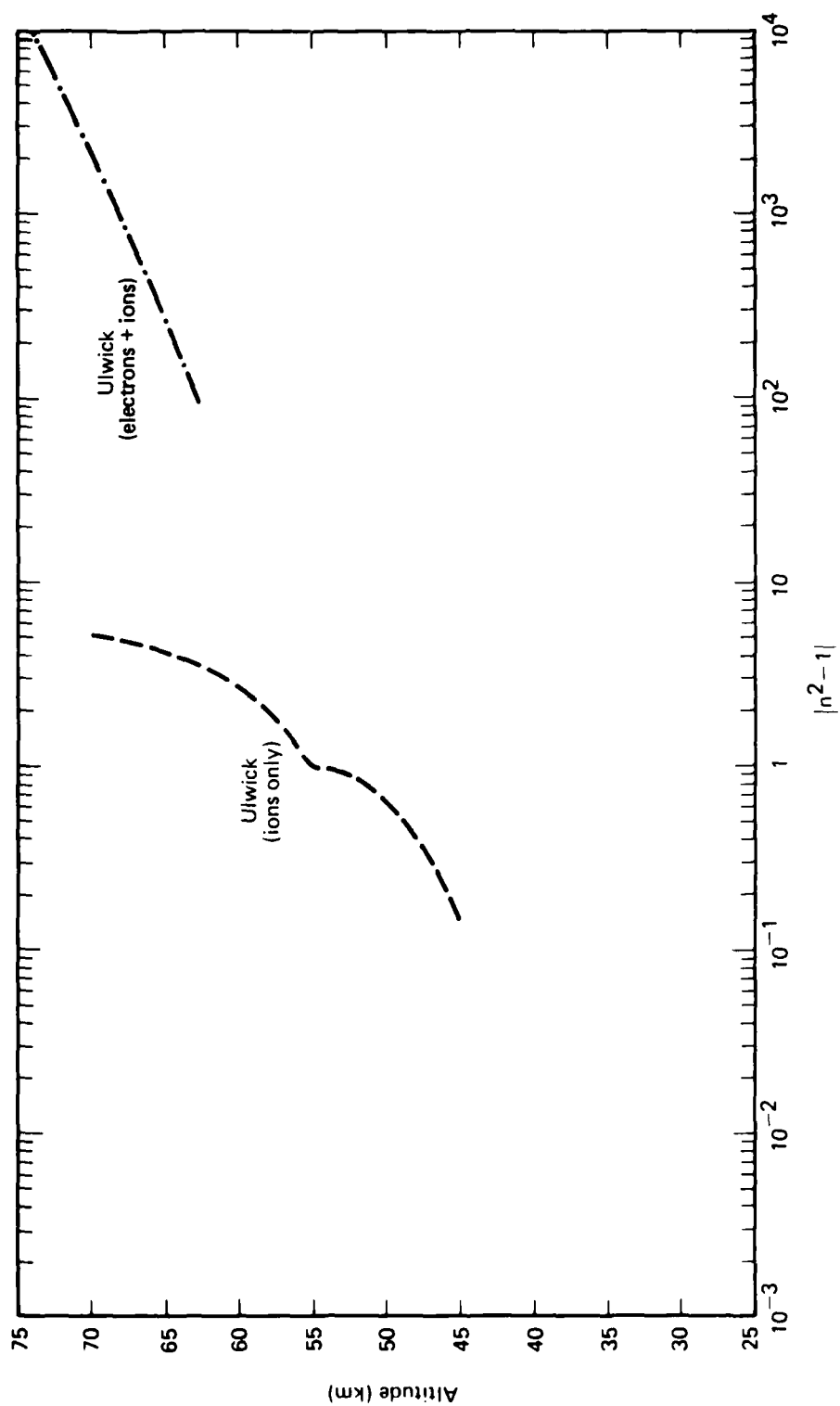
Figure 3.   Refractive-index height profiles at 75 Hz: sunset, 3 November 1969.

-18-

Several conclusions can be drawn from Table 1, or the equivalent Figs. 1 through 3:

1. Above 60 km or so, electrons dominate propagation because the total refractive index calculated from the conductivity data is much larger than that calculated from ions only.

2. At altitudes below about 55 km, the refractive index from Ulwick's data is somewhat smaller than that from the conductivity data. The difference could simply be due to scatter between two measurement methods, or could occur because the conductivity data include some electron contribution (as Hale et al. assert) whereas Ulwick's data do not.

3. Large gaps in the refractive index profiles occur at altitudes between about 60 km, above which electron density data are reliable; and 45 to 50 km, below which ions make the dominant contribution.

The third item above--the gaps in the refractive index profiles between about 50 and 60 km--probably causes the greatest uncertainty in interpreting ELF propagation experiments. Such gaps occur because electrons contribute strongly down to the altitude where $N_e \sim N^+/1500$. Since ion densities of a few tens of thousands per cubic centimeter are typical for PCA conditions (see Table 1), electron densities as small as a few tens of electrons per cubic centimeter must be measured for a good estimate of the refractive index. The data give electron densities no smaller than several hundred per cubic centimeter-- concentrations that occur near 60 to 65 km. Electron data are needed for altitudes perhaps 10 km lower, where--though much less numerous than ions--electrons are nevertheless the dominant influence.

Therefore, two types of uncertainties would have arisen if a coordinated rocket/ELF-propagation experiment had been performed during PCA 69. First, differences exist between refractive indexes obtained by alternative methods in the ion-dominated region, which includes most altitudes below ~50 km. Second, the interpolation of values in the refractive index between the ion-dominated region and the

-19-

lowest electron-dominated altitudes for which electron data are available is poorly defined.

To quantify these uncertainties, we have calculated ELF attenuation rates for the four refractive index profiles shown in Fig. 4. All profiles pertain to sunrise, 3 November 1969, and represent four models obtained by reasonable fits to the data plotted in Fig. 1. They are distinguished as follows:

- Profile A represents a sharp roll-off from the index based on Ulwick's data in the electron-dominated region to that based on his data in the lower altitude, ion-dominated region.

- Profile B represents a transition from the index based on Ulwick's data in the electron-dominated region to that based on the conductivity data of Hale et al. in the ion-dominated region.

- Profile C represents a gentle roll-off from the index based on Ulwick's data in the electron-dominated region to that based on his data in the ion-dominated region.

- Profile D is analogous to profile B, but was chosen to have a greater height gradient between altitudes of 40 to 50 km, which strongly affect ELF propagation.

Differences among the profiles are due to the inadequacies of the rocket data discussed above.

Table 2 lists attenuation rates in decibels per megameter of propagation calculated with PSR's long-wave propagation code using the profiles of Fig. 4. It also catalogs the calculated PCA-induced losses for the profiles, based on the assumptions that a 5 Mm length of propagation path is exposed to the PCA and that the ambient attenuation rate is 1.15 dB/Mm. A transpolar propagation experiment would be designed to measure such losses, which are the disparities between the received signals under ambient and PCA conditions. The differences among the computed losses result from both scatter in the rocket data and ambiguities in interpolating the refractive index through altitudes ranging from about 45 to 60 km.
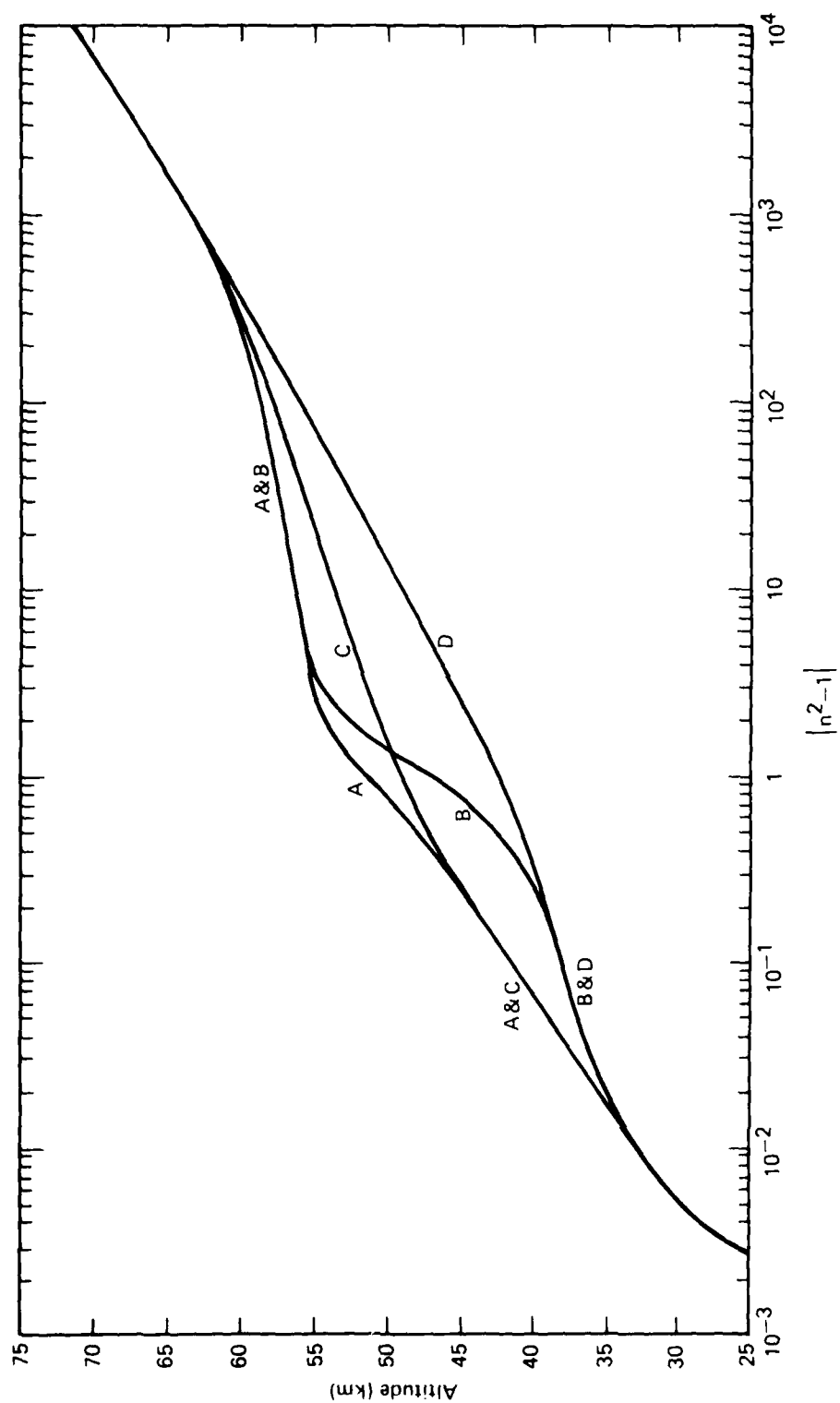
Figure 4. Model refractive-index height profiles at 75 Hz: sunrise, 3 November 1969.

-21-

Table 2. Calculated attenuation rates and
          PCA-induced signal losses for
          75 Hz and 5 Mm of exposed path.

Profile	Attenuation Rate (dB/Mm)	Signal Loss (dB)
A	1.5	1.75
B	1.8	3.25
C	1.35	1.0
D	1.5	1.75

For a useful comparison with experimental data, the computed results should exhibit a scatter significantly smaller than that of the PCA-induced loss. Unfortunately, Table 2 shows that the scatter is a large fraction of the expected signal loss. Strictly, this conclusion applies to only the *PCA 69* event. However, similar difficulties could be expected for any event where the accuracy and sensitivity of rocket-gathered measurements are no better than for *PCA 69*. Future experiments should concentrate on obtaining electron data down to altitudes of 50 km or even lower.

Should electron data prove unobtainable at such low altitudes with rocket-borne instruments, an alternative approach would be needed. One possibility is--applying atmospheric-chemical relations--to theoretically extrapolate measured electron densities to altitudes below 60 km. Another is to use satellite-borne sensors to measure fluxes of ionizing radiation incident on the ionosphere; then, using the chemical relations, to calculate the electron density at altitudes ranging from 45 to 60 km. Both alternatives are subject to uncertainties in the values of ionospheric reaction-rate coefficients.

-22-

SECTION 3

EFFECTS OF LATERAL IONOSPHERIC STRUCTURE ON ELF DURING PCA

The previous section considered the effects of vertical iono-
spheric structure on ELF propagation during a PCA. Here we consider
lateral ionospheric structure, which can influence ELF propagation for
two reasons. First, unlike conventional frequencies, ELF cannot be
analyzed solely in terms of ionospheric properties in the immediate
vicinity of the direct propagation path. Instead, ionospheric proper-
ties must be averaged over an ELF Fresnel zone, which can cover
millions of square kilometers for a transpolar path. Second, the
finite size of the polar cap must be taken into account.

SATELLITE DATA

Ideally, data on ionospheric height profiles at multiple dis-
persed locations are needed to determine the extent and uniformity of
a PCA-induced disturbance. To our knowledge, unfortunately, no co-
ordinated multiple-location measurements of ionospheric conductivity
or ionization have been taken during a major PCA. Even the extensive
rocket measurements during *PCA 69* were taken at one location. Thus,
data on the lateral structure of the earth-ionospheric waveguide
during a PCA must be gleaned from satellite measurements of incident
particle fluxes, which enhance ionization. Such a use of fluxes in-
stead of conductivity or density profiles introduces uncertainties
associated with the chemical calculations used to obtain the ioniza-
tion levels.

Reagan and Watt [1976] and Reagan et al. [1978] give data on
particle fluxes as functions of latitude for the PCAs of 3 August
1972 and 2 November 1969. Their data show proton and electron fluxes
measured in several energy bands as the satellites traversed the polar
cap at altitudes of several hundred kilometers. During the first half-
day of the 2 November 1969 event, the fluxes of 1.7, 13.0, and 24.5 MeV
protons exhibited spatial fluctuations up to about a factor of 3 within
the cap. No data were obtained for the 50 to 100 MeV protons, which

ionize the important 40 to 50 km region. Because data on the lower
altitudes are insufficient and the chemical coefficients are imprecise,
it is pointless to attempt a detailed calculation of the propagation
uncertainty due to the factor-of-3 spatial "jitter" in proton flux.
The ion density varies only as the square root of the production rate,
which is proportional to the incident flux. Thus, the spatial in-
homogeneity of the flux will probably cause no more than a factor of
2 inhomogeneity in the refractive index. As discussed below, addi-
tional variations will occur if reaction-rate coefficients are non-
uniform across the cap.

Spatial variations in proton flux seem to diminish as the PCA
develops. Data taken on 3 November 1969 indicate a more uniform flux
than that for 2 November. Moreover, data given by Reagan and Watt
[1976] show that proton fluxes measured at several energies between
1 and 100 MeV were quite uniform across the cap on 4 August 1972--the
second day of that event.

These few measurements indicate that only slight lateral in-
homogeneities in the refractive index are caused by inhomogeneities
in proton flux once a PCA has had a day to develop. Even earlier,
the refractive index inhomogeneity due to flux inhomogeneity is prob-
ably no worse than a factor of 2. Sensitivity studies show that no
intolerable uncertainties in predicted ELF signal strengths would
occur even if the conductivity height profile were uncertain by a
factor of 2 over the entire first Fresnel zone. In fact, the satel-
lite data indicate that transverse variations in proton flux have
characteristic scales of only hundreds of kilometers, and would be
averaged over the enormous ELF Fresnel zones (see Figs. 5 and 6 below).

Having discussed inhomogeneities due to lateral structure in the
proton flux--i.e., those that would occur even if reaction-rate coef-
ficients were uniform across the cap--we conclude that, in the two PCAs
examined, such inhomogeneities apparently would not have seriously
degraded the interpretation of a transpolar ELF propagation experi-
ment. However, lateral inhomogeneities can be caused by another
mechanism. The chemical coefficients governing ionization caused by
a given proton flux could vary across the cap. If such a variation

were large, lateral gradients in the refractive index could result even
if the flux were spatially uniform. To evaluate the implications of
such chemistry-induced inhomogeneities, air chemistry research must
estimate the variation of key reaction-rate coefficients across the
cap.

EFFECT OF POLAR CAP BOUNDARY ON ELF PROPAGATION

Since transpolar ELF propagation depends on the size of the
proton-irradiated region, it is affected by polar cap boundary vari-
ability. Satellite data on the geographic dependence of the proton
flux are given by Imhoff et al. [1976]. For the energetic protons
of interest here, the effective boundary of the cap typically occurs
within invariant latitudes of 65 deg ± 5 deg; i.e., the linear dimen-
sions of the cap vary up to about 5 deg/(90 deg – 65 deg) ~ 20 per-
cent, whereas the corresponding area varies up to about 40 percent.

Figures 5 and 6 show the first Fresnel zone for 75 Hz propagation
from WTF to Tromsö and Thule, respectively. The shaded area is the
region irradiated by energetic protons at 1400 UT on 4 August 1972
[Imhoff et al., 1976]. As noted above, the boundaries of the polar
cap can vary by a few degrees in latitude. Here we investigate the
sensitivity of transpolar propagation to the location of the effective
boundaries.

It is convenient to characterize polar-cap-boundary effects as
either longitudinal or transverse. Longitudinal effects depend on
the length of the great-circle propagation path exposed to the PCA,
whereas transverse effects depend on the fraction of the Fresnel-zone
cross section filled by the PCA. For a laterally uniform cap with
sharp boundaries, longitudinal effects are governed by the intersec-
tions of the cap boundary with the great-circle propagation path
(see Figs. 5 and 6); transverse effects are governed by the inter-
sections of the boundary with the line that normally bisects the great-
circle path and terminates at the widest points of the first Fresnel
zone. The length of this line is 2d, where

$$d = \frac{1}{2} \left(\frac{x\lambda}{S_0} \right)^{1/2} \tag{9}$$

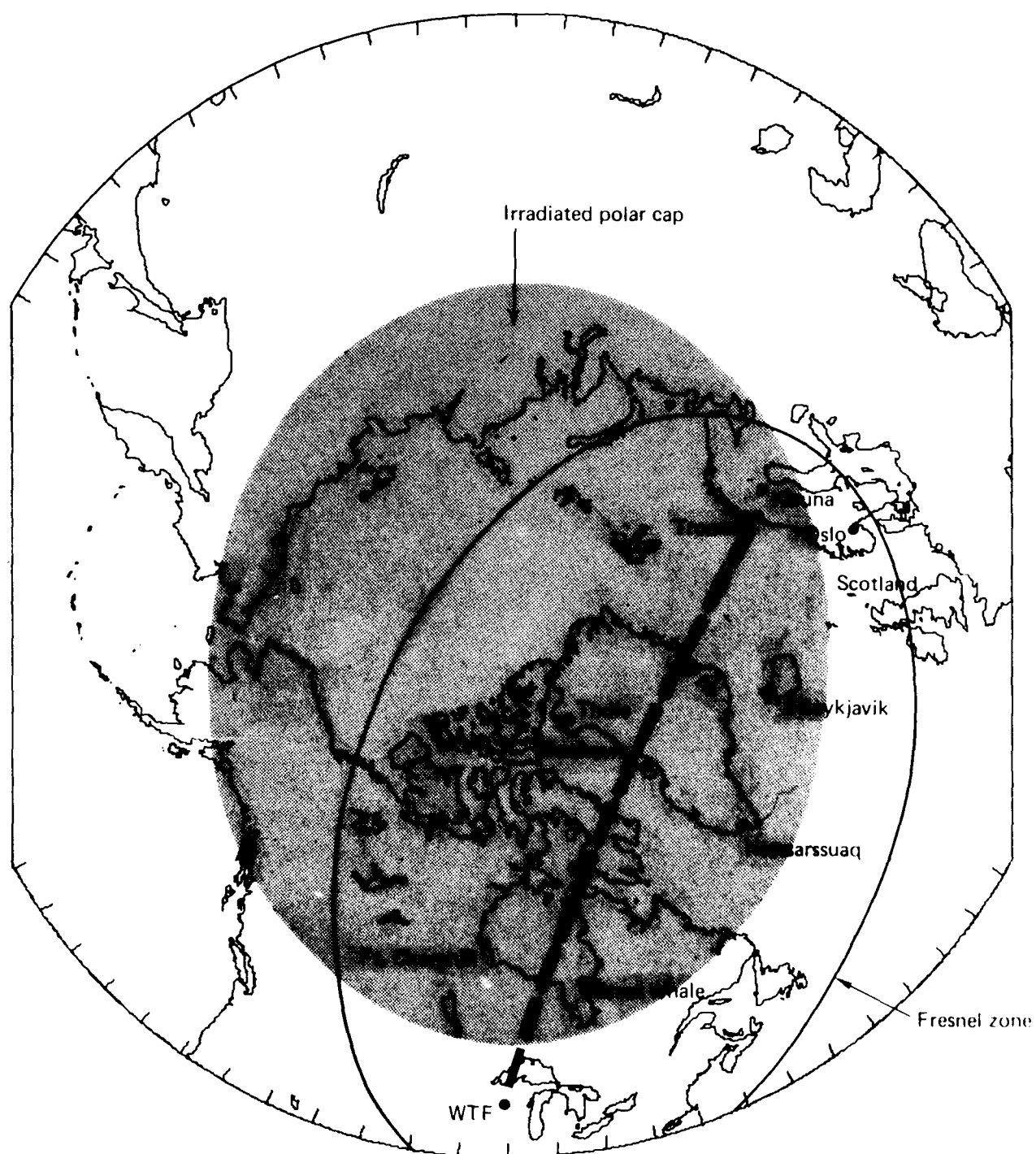-25-

Irradiated polar cap

Fresnel zone

Scotland

Reykjavik

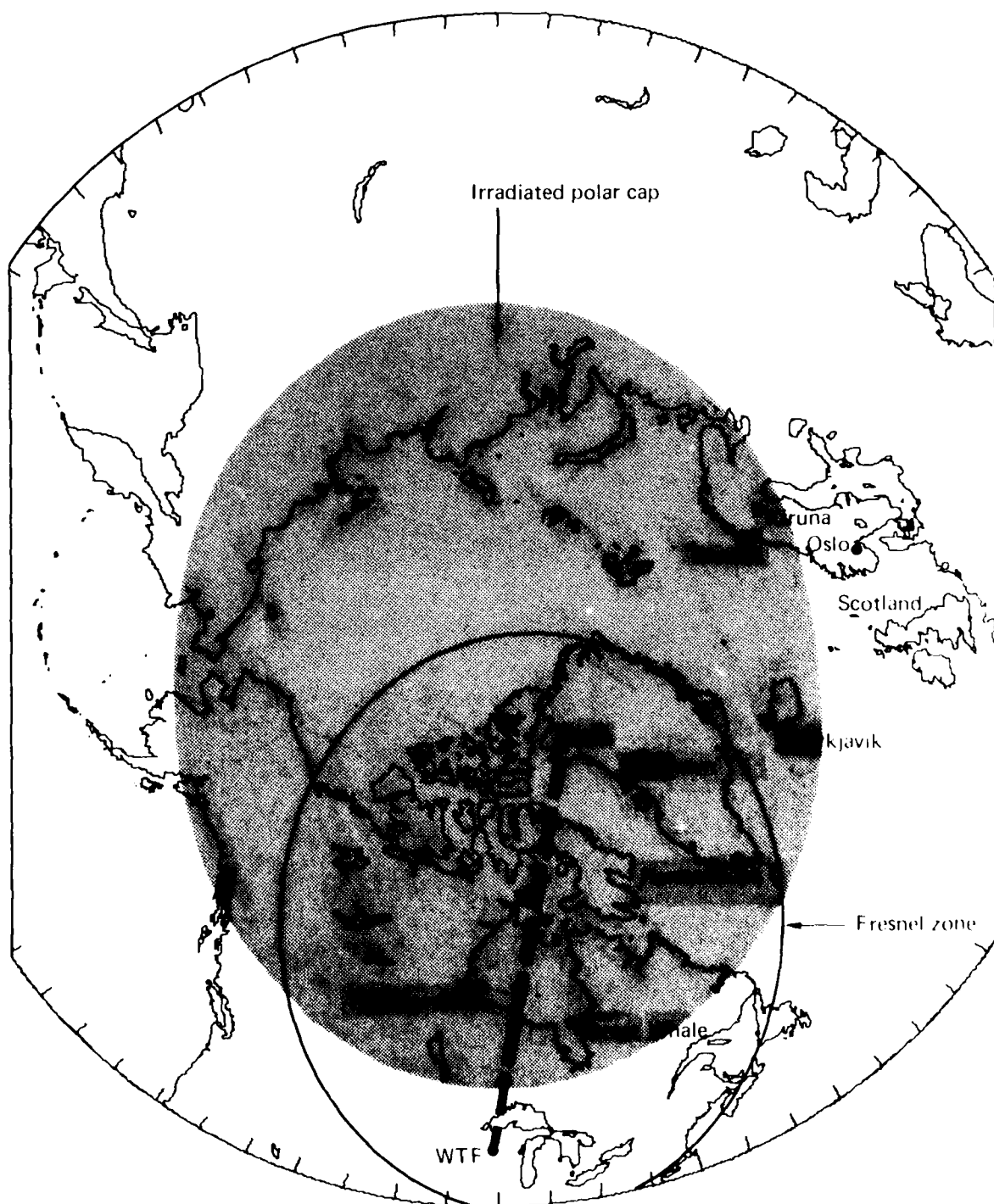Narssuaq

WTF

Figure 5. Fresnel zone at 75 Hz for WTF-to-Tromsö path.

Figure 6. Fresnel zone at 75 Hz for WTF-to-Italy path.

is the maximum half-width of the Fresnel zone, x is the great-circle pathlength, λ is the wavelength, and the propagation constant $S_0 \sim$ 1.15 to 1.5 for 75 Hz propagation

Longitudinal boundary effects are relatively straightforward to analyze. For example, consider the paths from the WTF to Tromsö and Thule in Figs. 5 and 6. We assume--subject to later deliberation-- that (1) the cap fills the Fresnel-zone cross section, so transverse effects are minimal; and (2) the transmitter is outside the cap's boundaries and the receiver is within. The latter assumption is valid for the WTF-to-Thule path, but could be violated for WTF-to-Tromsö should the boundary occur at a latitude higher than indicated in Fig. 5.

Subject to these assumptions, uncertainties in the boundary location can affect only the PCA-induced attenuation A (but not the excitation), which is given by

$$A = (\beta - \beta_0)L \quad dB , \tag{10}$$

where β is the attenuation rate under the disturbed cap, β_0 is the ambient attenuation rate, and L is the exposed pathlength. The fractional uncertainty in attenuation $\Delta A/A$ caused by an uncertainty in exposed pathlength ΔL, due to an imprecisely known boundary location, is simply

$$\frac{\Delta A}{A} \approx \frac{\Delta L}{L} . \tag{11}$$

In short, without continuously monitoring the extent of the cap, the boundary location can be estimated to within ± 5 deg of latitude, i.e., to within about ± 500 km. $L \approx 5$ Mm for a transpolar path such as WTF to Tromsö, and about 2.5 Mm for WTF to Thule. The corresponding fractional uncertainties in PCA-induced attenuation are $+10$ and $+20$ percent, respectively. The absolute value of the longitudinal effect of a 500 km uncertainty in boundary location would be about $+0.5$ dB uncertainty in calculated field strength for a relatively strong event (1 dB/Mm excess attenuation). These numbers could double if the receiver were outside the cap, because boundary errors would occur at each end of the path.

A more important error could result if the receiver were so near the boundary that it was uncertain whether the disturbed or ambient value should be used for the excitation factor. For a strong event, the difference between ambient and disturbed excitation at the receiver could be ~1.5 dB [Field, 1969]. Thus, the status of the receiver site must be established either by sounding the ionosphere or locating the receiver so that no reasonable doubt exists as to whether it is inside or outside the irradiated cap.

Transverse effects are more complicated than longitudinal; they can be analyzed with either scattering theory or the integral wave equation. Field and Joiner [1979] used the latter approach to obtain results that, although not derived explicitly for a polar cap model, clarify the problem at hand. Specifically, Field considered a disturbance having the transverse dependence

$$e^{-y^2/(\Delta y)^2} ,$$

where y is the distance from the direct propagation path and Δy is a measure of the transverse size of the disturbance. It was shown that the ratio R of the actual field-strength reduction to that computed by assuming the disturbance to be infinitely wide (i.e., by using the WKB approximation and thus ignoring transverse gradients) is simply

$$R = \left[1 - \frac{i}{\pi} \left(\frac{d}{\Delta y} \right)^2 \right]^{-1/2} . \tag{12}$$

If the disturbance is wider than a Fresnel zone (d/$\Delta y \ll 1$), then R → 1, the effects of finite transverse size are negligible, and the WKB result is recovered. For $\Delta y \underset{\sim}{<} d$, R is smaller than unity, indicating that PCA-induced attenuation computed including transverse effects is less than that computed by simply integrating along the direct path (e.g., as in Eq. (10)).

Figure 7 shows R as a function of Δy and $\Delta y/d$ for a 6 Mm path and frequencies of 45 Hz and 75 Hz. Transverse effects would be negligible--and the transverse location of the cap boundaries unimportant--if $|R|$ were unity and the phase of R were zero. If the disturbance fills at least 75 percent of the Fresnel-zone cross section, then $|R| > 0.9$ and phase R < 10 deg, which indicates that boundary effects are unimportant if $\Delta y/d > 0.75$. Figures 5 and 6 demonstrate that, for the paths shown, more than 80 percent of the Fresnel-zone cross section is filled. The error made by ignoring edge effects is about 5 percent (Fig. 7). Of course, transverse boundary effects could be much greater for other paths--e.g., $\Delta y/d$ would be about 0.5 for WTF to Scotland. In such cases, the location of the cap boundary must be known to correctly calculate the signal. The simplest procedure would be to avoid paths passing near the edge of the cap and ignore transverse boundary effects.
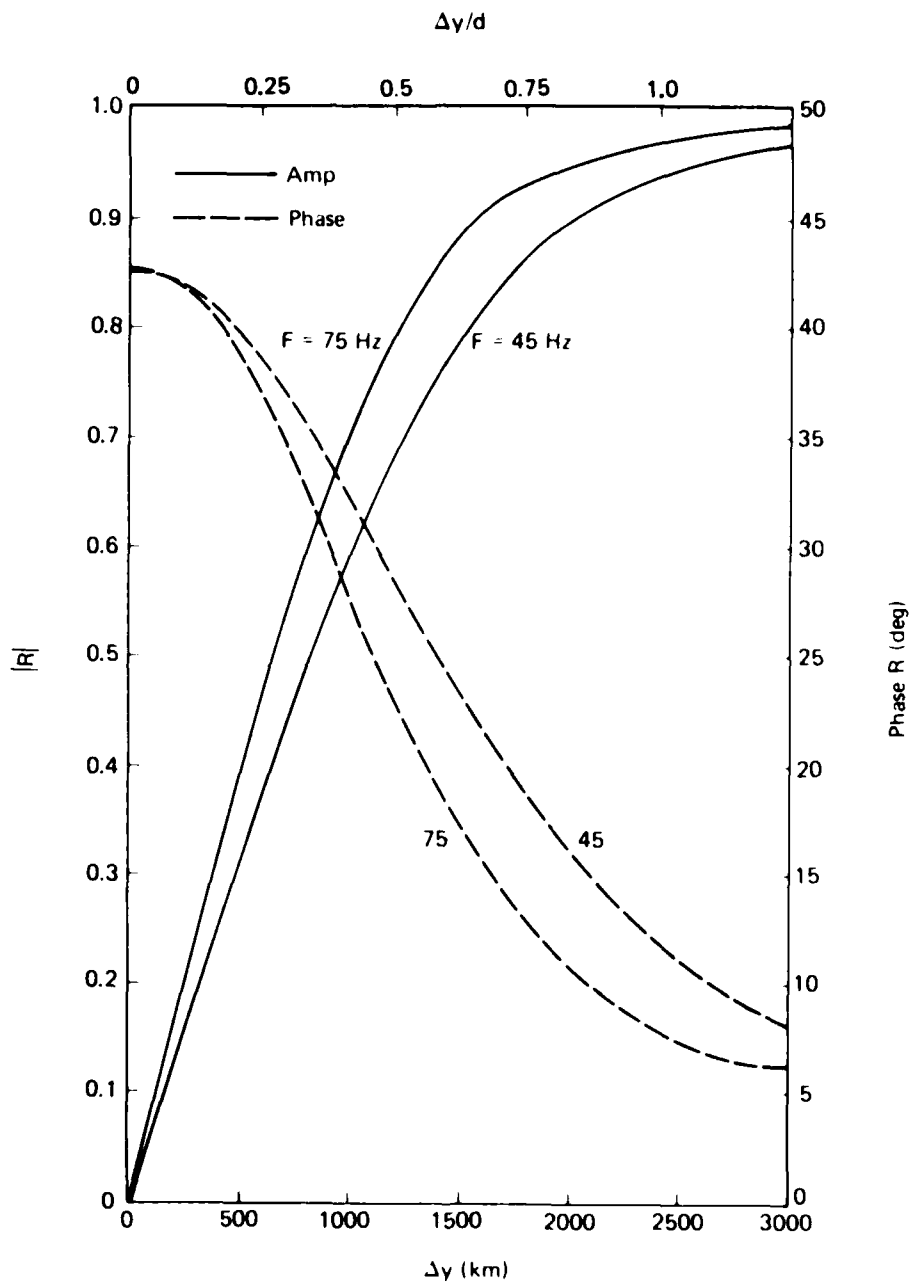
Note: d = Fresnel zone half-width, Δy = effective half-width of disturbance

Figure 7. Ratio of actual propagation anomaly to that computed
ignoring transverse boundary effects.

SECTION 4

SIGNAL AND NOISE PROCESSING

Here we establish the amount of signal and noise processing needed
to accurately estimate the transpolar WTF signal. The tradeoff is
difficult because the signal integration time must be long enough to
yield a good postprocessing signal-to-noise ratio (SNR), but short
relative to temporal changes in a PCA. One troublesome aspect is
that strong PCAs--which best simulate nuclear environments--cause
the lowest SNRs and thus require the longest integrations. After
estimating atmospheric noise and the expected ambient and disturbed
signal strengths at two possible receiver sites, we determine the
integration times needed to resolve the PCA-induced change in signal
amplitude.

EXPECTED SIGNAL AND NOISE

We assume that the WTF signal will be received at Thule, Greenland,
and Tromsö, Norway, whose positions are shown in Figs. 5 and 6. We
consider a signal frequency of 75 Hz, and characterize the WTF trans-
mitter by a horizontal dipole with a length ℓ of 22.5 km and current
I of 300 A terminated in ground with a conductivity σ_g of 6×10^{-4}
mhos/m. For this estimate, we characterize the earth-ionosphere wave-
guide by an attenuation constant α; a relative phase velocity factor
c/v_{ph}, where c is the speed of light; and an effective ionospheric
height h. Table 3 lists assumed values for these parameters under
normal and disturbed (PCA) conditions. Values for disturbed condi-
tions correspond to a very strong PCA; less severe deviation from
ambient would be expected for smaller, more common events (e.g.,
Field [1969]).

The magnetic intensity H can be calculated from these parameters
with the expression (e.g., Bannister [1974]):

Table 3. Assumed waveguide parameters.

Parameter	Normal	Disturbed
α	0.132 nep/Mm (1.15 dB/Mm)	0.29 nep/Mm (2.5 dB/Mm)
c/v_{ph}	1.15	1.4
h	50 km	40 km

$$|H| = \frac{If}{240\pi}\left(\frac{2\pi\mu_0}{c}\right)^{1/2} \frac{e^{-\alpha D}}{h_g^{1/2}\ (a\ \sin\ D/a)^{1/2}\ (c/v_{ph})^{1/2}} \quad A/m\ , \quad (13)$$

which, after substituting values for physical constants, becomes

$$|H| = 1.76 \times 10^{-3}\ \frac{1}{h}\ \frac{e^{-\alpha D}}{\left[(c/v_{ph})\ \sin\ D/a\right]^{1/2}} \quad A/m\ , \quad (14)$$

where f is the frequency, a is the earth's radius, and D is the distance from the transmitter.

The value of h to be used in Eq. (14) is the geometric mean of the effective height of the ionosphere at the transmitter and receiver. The WTF is at too low a geomagnetic latitude to be affected by a PCA. Tromsö, on the other hand, is located such that the ionospheric height could be depressed, depending on the details of the PCA (e.g., development of ring current).

Table 4 lists calculated signal amplitudes at Tromsö and Thule under normal and disturbed conditions, assuming the ionosphere to be depressed at those locations but not at WTF. We see that a very large event can cause a signal reduction of about 8 dB at Tromsö and 5 dB at Thule. Moderate events will cause a 4 to 5 dB reduction at Tromsö.

Table 4. Calculated signal amplitudes.

Location	Normal (dBH)	Disturbed (dBH)
Tromsö	-156	-164
Thule	-150	-155

NOTE: Values are in decibels relative to 1 A/m.

Evans and Griffiths [1974] as well as Davis and Myers [1976] report measurements of effective atmospheric noise in Norway after excision or clipping of the larger impulses. The former cite a median of -143 dBH, with lows of -148 dBH and highs of -138 dBH. They observed a diurnal variation and found a 2 dB decrease in noise in the early morning in Norway. Davis and Myers [1976], who investigated impulse clipping at various levels, record slightly higher effective noise levels, with a median of nearly -141 dBH during the summer in Norway. They estimate that processing reduced effective noise by over 10 dB. Without noise processing, therefore, their measured level would have been about -130 dBH.

We compromise between the above measurements, using -142 dBH for the expected atmospheric noise level at the receiver if clipping is used. We estimate noise to be 10 dB higher in the absence of clipping. Table 5 shows expected signal-to-noise ratios obtained by combining these noise levels with the signal strengths shown in Table 4. We have used the same noise levels for ambient and disturbed conditions at Tromsö, which is near the edge of the polar cap and so receives atmospheric noise via nonpolar propagation paths from most thunderstorm centers. Thule, on the other hand, is well within the cap, and we have assumed that a PCA would suppress signal and noise about equally. Thus, the disturbed and undisturbed SNRs are taken to be the same there.

Table 5. Expected SNRs under normal and disturbed conditions.

Location	Normal (dB)		Disturbed (dB)	
	Clipped Noise	Unclipped Noise	Clipped Noise	Unclipped Noise
Tromsö	-14	-24	-22	-32
Thule	-8	-18	-8	-18

NOTE: Values pertain to a 1 Hz bandwidth.

INTEGRATION OF SIGNAL

For verifying the predictive codes, the signal must be measured precisely enough to resolve the change caused by a PCA. For a very strong event, Table 4 shows that an 8 dB decrease in the signal would be expected at Tromsö. In such a case, the signal would have to be measured to within about 2 dB before and during the event. The measurement during the event is the more difficult, because of the reduced SNR. Events small enough to cause a signal reduction of just a few decibels would require measurement precision of 1 dB or less. However, that necessity is partially mitigated by the greater SNR during a moderate than a severe event.

Table 5 shows SNR in a 1 Hz bandwidth, which is equivalent to a 1 sec integration time. Since these ratios are very low, integration times much longer than 1 sec are needed to measure the signal with acceptable statistical stability. Two kinds of integration can be considered--coherent and noncoherent. Coherent integration requires that signal phase be constant over the period of integration, or, alternatively, that estimates of phase be available so variations can be compensated. The usual practice is to integrate coherently as long as possible, subject to both conditions regarding phase, then integrate noncoherently for further improvement in postprocessing SNR. During the period of coherent integration, the SNR increases linearly with time. Noncoherent integration improves SNR at a lesser rate-- a rule of thumb being that the improvement is proportional to the square root of the integration time. Here we estimate the expected SNR somewhat more accurately.

We first assume that the signal is integrated coherently and compute the likelihood that noise causes the measured signal to exceed the expected signal by various amounts. Specifically, we compute the power level that would be exceeded by chance on no more than 10 percent of independent attempts to measure the signal under specific conditions.

That likelihood can be expressed in terms of the noncentral chi-square distribution with two degrees of freedom. Let the expected complex signal amplitude be $r\sigma\, e^{i\phi} = m_x + m_y$, where the noise is uniformly distributed in phase ϕ with standard deviation σ. The likelihood that a measurement of the power would be equal to or less than $R^2\sigma^2$ is given by the integral

$$\iint_A (2\pi\sigma^2)^{-1}\ \exp\left[-\ \frac{(x - m_x)^2 + (y - m_y)^2}{2\sigma^2}\right] dx\ dy = P(R^2|2,\ r^2)\ ,$$

(15)

where A denotes the area of a circle of radius $R\sigma$ centered at the origin, and $P(R^2|2,\ r^2)$ is the cumulative distribution function of the noncentral chi-square distribution with two degrees of freedom and noncentrality parameter r^2. In Eq. (15), we may identify r^2 as the expected SNR in a 1 Hz bandwidth and R^2 as the corresponding power realized in a measurement.

If σ is the rms noise amplitude in a 1 Hz bandwidth, the rms noise amplitude resulting from T sec of coherent integration would be $\sigma\sqrt{T}$, whereas the integrated signal amplitude would be

$$r\sigma T\, e^{i\phi} = m_x T + i m_y T\ .$$

The likelihood that the integrated measurement would indicate a power no greater than $R^2\sigma^2 T^2$ is, by analogy with Eq. (15), given by

$$\iint_A (2\pi\sigma^2 T)^{-1} \exp\left[-\frac{(x - m_x T)^2 + (y - m_y T)^2}{2\sigma^2 T}\right] dx\, dy = P(R^2 T | 2,\ r^2 T) ,$$

(16)

where A is now the area within a circle of radius $R\sigma T$.

Tables of the noncentral chi-square distribution $P(x^2 | \nu,\ \lambda)$ are available. For x^2 and λ large (>3), however, the cumulative distribution function can be approximated with the normal distribution function:

$$P(x^2 | \nu,\ \lambda) \approx P(x) = \frac{1}{\sqrt{2\pi}} \int_{-\infty}^{x} e^{-t^2} dt ,$$

(17)

where

$$x = \frac{(x^2/g)^{1/3} - \left[1 - \frac{2}{9}\left(\frac{1 + b}{g}\right)\right]}{\sqrt{\frac{2}{9}\,(1 + b)/g}} ,$$

(18)

and where $g = \nu + \lambda$ and $b = \lambda/g$ [Abramowitz and Stegun, 1972]. Equations (16) through (18) were used to compute Fig. 8, which shows, for $P(R^2 T | 2,\ r^2 T) = 0.9$, how R^2 approaches r^2 with increasing coherent integration time T. The SNR ratio in a 1 Hz bandwidth is shown parametrically on the curves.

Figure 8 shows envelopes of 90 percent confidence that the ratio R/r of the measured signal to the mean signal will not be greater than shown on the ordinate. A set of similar curves would show the envelopes of 90 percent confidence that the inverse of this ratio will not be greater than shown on the ordinate. The curves on Fig. 8 show envelopes of 80 percent confidence that the quantity $|20 \log R/r|$ will thus not be greater than the amount indicated.

To illustrate the use of Fig. 8, consider normal conditions at Tromsö with noise clipping (SNR = -14 dB from Table 5). The figure
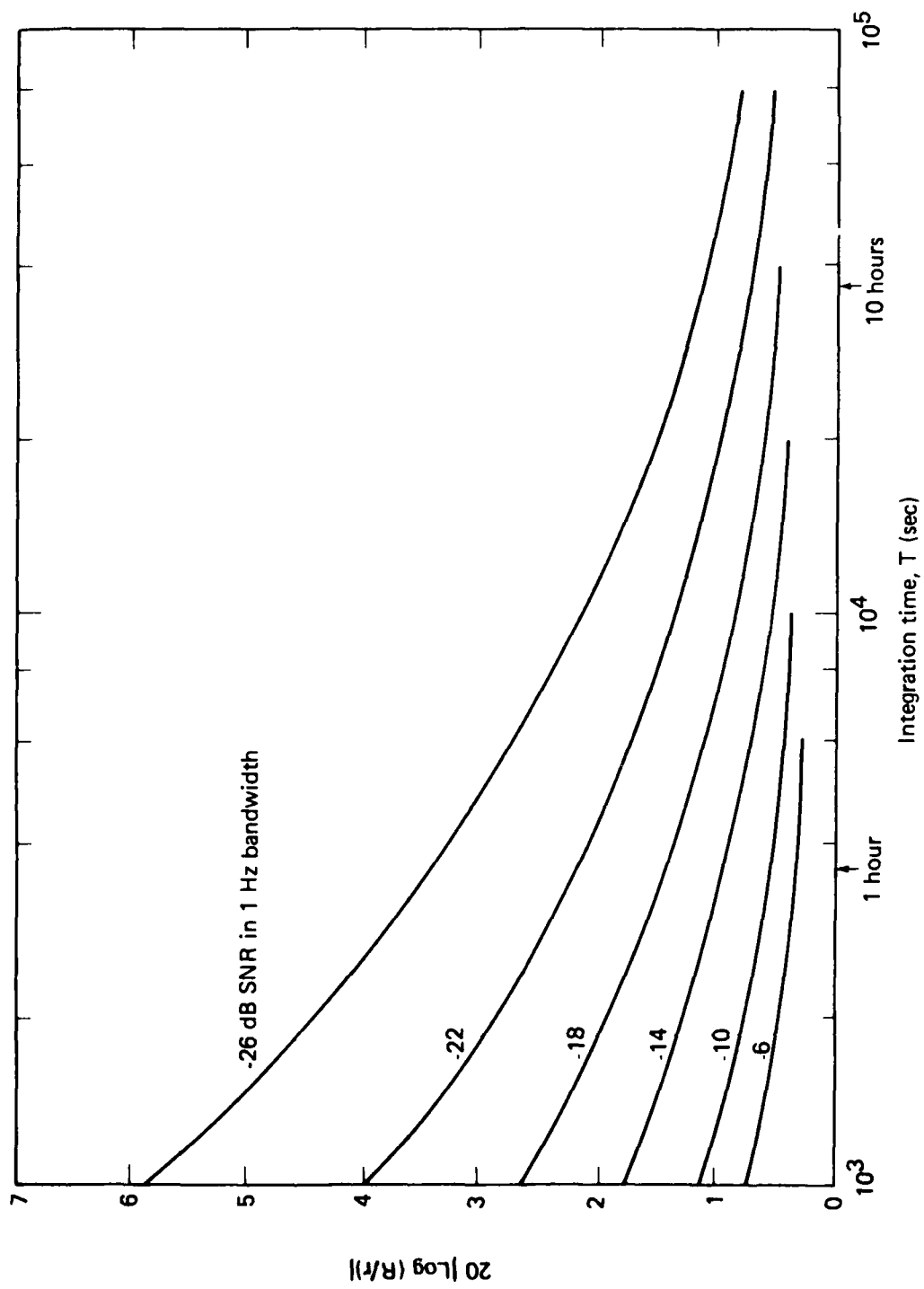
Figure 8. 80 percent confidence levels versus coherent integration time.

-83-

shows that 1 hr of coherent integration would give 80 percent confidence that the measured signal is within ±1 dB of the mean signal. For highly disturbed conditions at Tromsö with noise clipping (SNR = -22 dB from Table 5), Fig. 8 shows that 2×10^4 sec (about 5.5 hr) of coherent integration is needed to achieve ±1 dB accuracy with 80 percent confidence. The importance of noise clipping is demonstrated by using SNRs for unclipped noise from Table 5 in conjunction with Fig. 8. For normal conditions at Tromsö (SNR = -24 dB), nearly 10 hr of coherent integration is needed for 80 percent confidence of ±1 dB accuracy. For disturbed conditions (SNR = -32 dB), the requirements are so severe that the 80 percent confidence envelope is off-scale on Fig. 8. Thus noise clipping is essential.

This theory is valid either if the signal phase is constant, or if its variation is known and can be compensated. Less efficient non-coherent integration must be used if neither condition is met. In such a case, coherent integration would be employed as long as possible--e.g., as long as phase could be assumed to vary by less than, say, 1 rad; or as long as permitted by the particular receiver used. At the end of each such interval, the coherently integrated power would be measured; and the results of some number N of such measurements would be averaged to obtain a single estimate of the received power.

If the complex amplitude of the kth measurement of the coherently integrated signal (plus noise) is $X_k + iY_k$, the result of summing the power for N such measurements is

$$x^2 = \sum_{k=1}^{N} (X_k^2 + Y_k^2) \ .$$

This summation again has a noncentral chi-square distribution, but now with 2N degrees of freedom. The likelihood that the averaged power measurements do not exceed R^2 is thus given by $P(R^2 T_c | 2N, \ r^2 T_c)$, where T_c is the duration of the coherent integration and N is the number of coherent measurements; i.e., $N = T/T_c$.

Figure 9, analogous to Fig. 8, shows the 80 percent confidence envelopes for noncoherent averaging of measurements made with hour-long coherent integrations.* Note that, for a given integration time, the signal uncertainty indicated in Fig. 9 is somewhat greater than that shown in Fig. 8 for coherent integration.

Figure 10 presents the information from Fig. 9 so as to illustrate the effect of integration time on resolution of changes in received power. The horizontal lines correspond to mean SNR in a 1 Hz bandwidth, whereas the shaded regions surrounding each line give the 80 percent confidence envelopes. The labels on the horizontal lines correspond to the values for clipped noise given in Table 5.

Consider, for example, a receiver at Tromsö where the mean ambient SNR (in 1 Hz) is -14 dB. A very strong PCA would change it to -22 dB-- an 8 dB separation between the disturbed and undisturbed values. Statistically valid resolution of that change requires an integration time long enough that the 80 percent confidence values corresponding to the two mean signal levels are well separated. The graph shows that 3 hr ($\sim10^4$ sec) of integration would resolve the normal signal to within ±0.6 dB with 80 percent confidence, and the disturbed signal to within ±1.6 dB. The resulting ~2 dB uncertainty in the difference between the disturbed and undisturbed signals is probably tolerable for an "8 dB" event.

Much longer integration times are needed to resolve smaller events. Consider, for example, a moderate "4 dB" PCA that reduces the mean Tromsö SNR from -14 to -18 dB. A 10^4 sec integration would result in a ±1 dB uncertainty in disturbed signal. Combined with the ±0.6 dB uncertainty in normal signal, that value would yield a total uncertainty of ~1.6 dB--40 percent as large as the 4 dB change being monitored, and probably too large for code verification. A total uncertainty less than, say, 1 dB would be acceptable in this case.

Figure 10 shows that an integration time of nearly 10 hr would be needed to achieve ±0.6 dB and ±0.2 dB uncertainty on the disturbed

_____

*This choice of coherent integration time is compatible with the capabilities of receivers considered for the experiment.
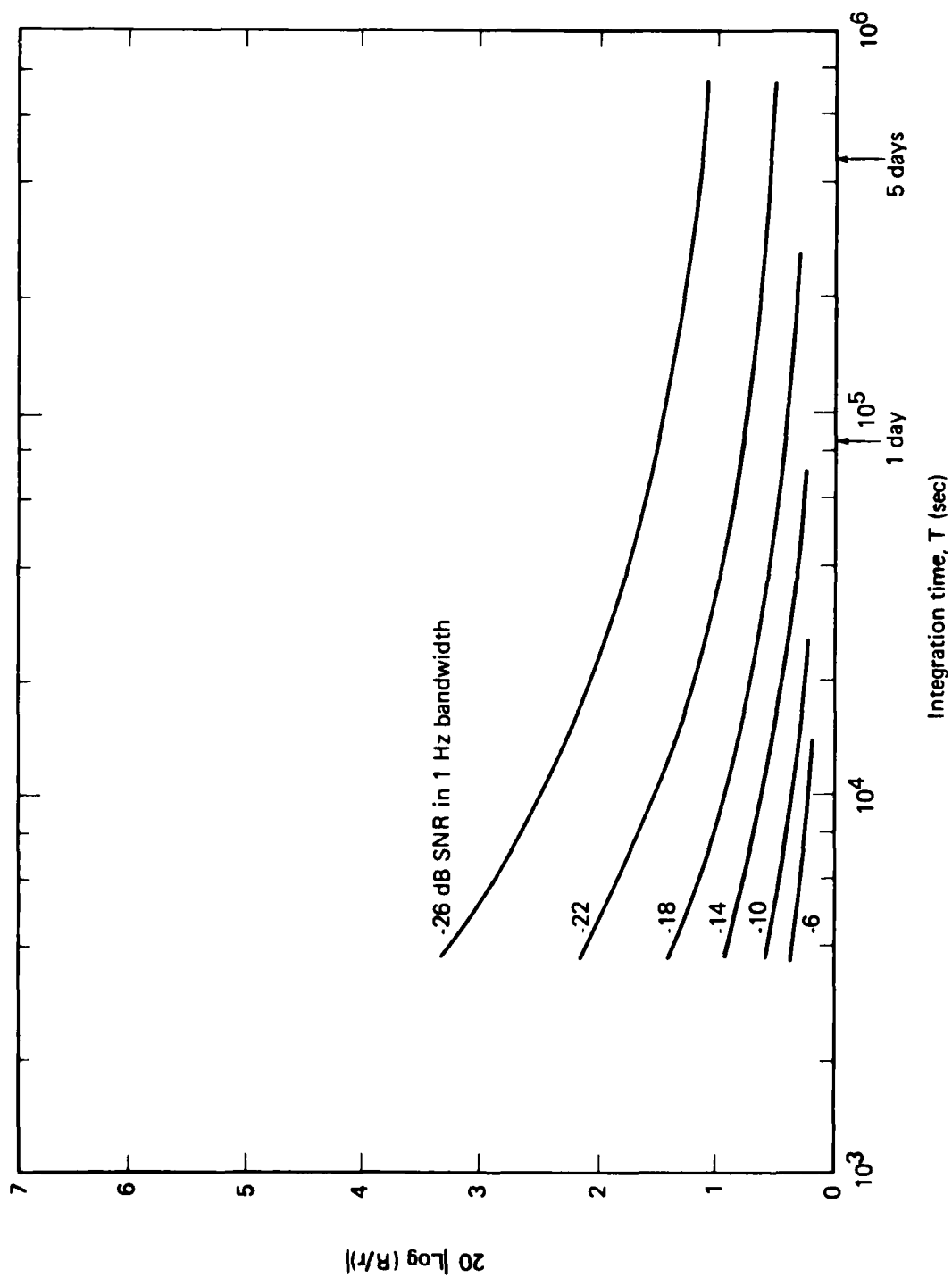
Figure 9. 80 percent confidence levels versus time: noncoherent integration of hour-long coherently integrated samples.
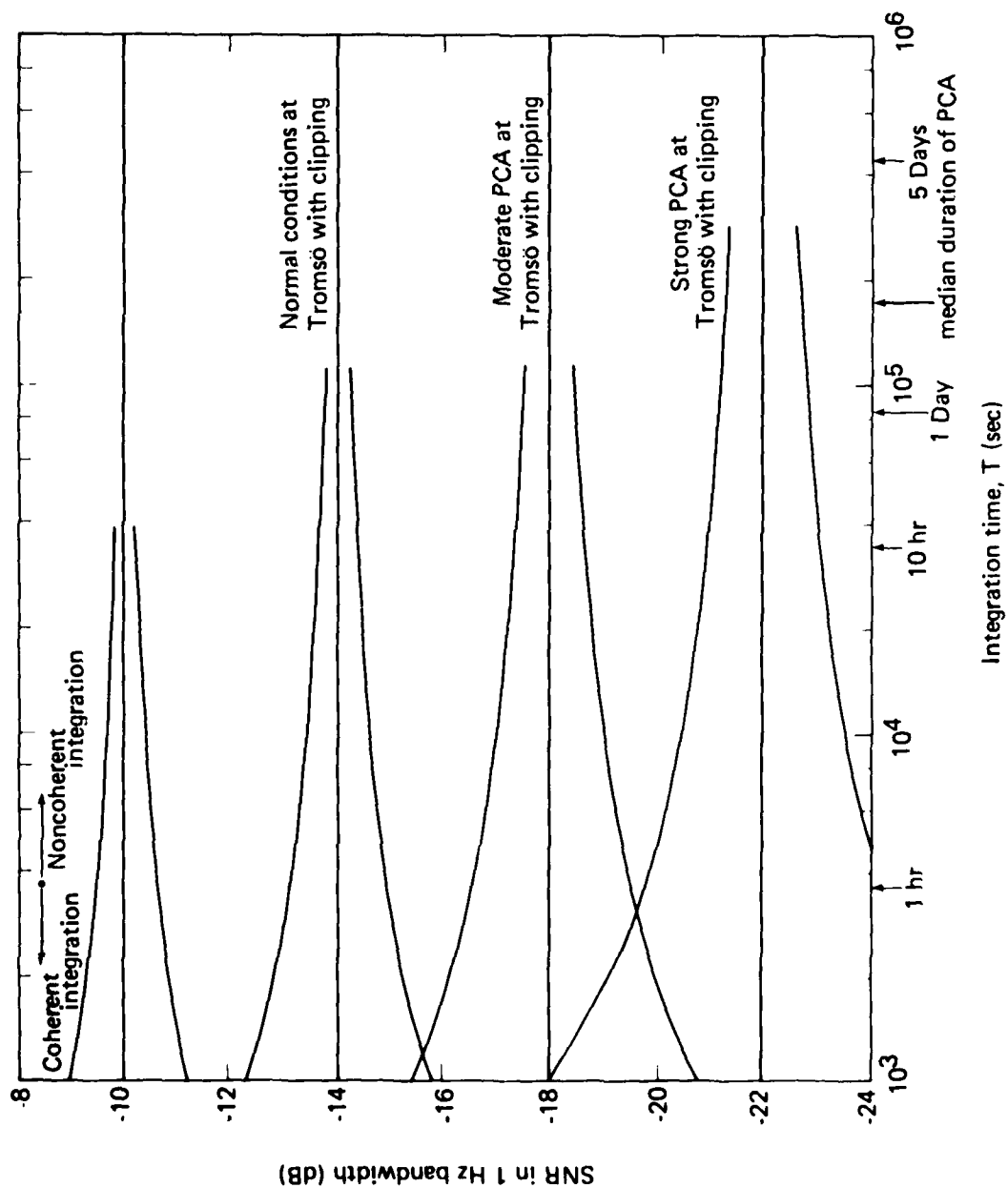
Figure 10. 80 percent confidence envelopes versus time: noncoherent integration of hour-long coherently integrated samples.

and normal signals, respectively. Such long times are troublesome because the ionosphere--and, hence, the signal level--could well change during the measurement. Figure 9 shows that some reduction in the integration time would be possible if coherent integration could be used throughout the entire measurement. Otherwise, a relatively strong event is needed if a statistically reliable measurement of the change in signal level is to be obtained.

REFERENCES

Abramowitz, M., and I. A. Stegun, *Handbook of Mathematical Functions*, National Bureau of Standards, Applied Mathematics Series 55, December 1972.

Bannister, P. R., "Far-Field Extremely Low Frequency (ELF) Propagation Measurements, 1970-1972," *IEEE Trans. Commun.*, Vol. COM-22, April 1974, p. 468.

Davis, J. R., and W. D. Myers, "ELF Atmospheric Noise Excision by Wideband Clipping," *Radio Sci.*, Vol. 11, December 1976, p. 991.

Evans, J. E., and A. S. Griffiths, "Design of a Sanguine Noise Processor Based upon World-Wide Extremely Low Frequency (ELF) Recordings," *IEEE Trans. Commun.*, Vol. COM-22, April 1974, p. 528.

Field, E. C., "Propagation of ELF Waves under Normal and Naturally Disturbed Conditions," *J. Geophys. Res.*, Vol. 74, 1 July 1969, p. 3639.

Field, E. C., *ELF Propagation under Disturbed Conditions: Comparison of Theory with Available Data*, Pacific-Sierra Research Corporation, DNA 4700F, 1 December 1978.

Field, E. C., C. Greifinger, and K. Schwartz, "Transpolar Propagation of Long Radio Waves," *J. Geophys. Res.*, Vol. 77, 1 March 1972, p. 1264.

Field, E. C., and R. G. Joiner, "An Integral-Equation Approach to Long-Wave Propagation in a Nonstratified Earth-Ionosphere Waveguide," *Radio Sci.*, Vol. 14, November-December 1979, pp. 1057-1068.

Hale, L. C., J. R. Mentzer, and L. C. Nickell, "Blunt Probe Measurements during a PCA Event," Chap. 22 in J. C. Ulwick (ed.), *Proceedings of COSPAR Symposium on Solar Particle Event of November 1969*, Air Force Cambridge Research Laboratories, AFCRL-72-0474, 11 August 1972, pp. 333-340.

Imhoff, W. L., et al., *Analysis of Satellite Data on Precipitating Particles in Coordination with ELF Propagation Anomalies*, Lockheed Missiles and Space Company, LMSC-D-50206, 30 April 1976.

Knapp, W. S., and K. Schwartz, *Aids for the Study of Electromagnetic Blackout*, General Electric/TEMPO, DNA 3499, 1 February 1975.

Proceedings of COSPAR Symposium on Solar Particle Event of November 1969, Air Force Cambridge Research Laboratories, AFCRL-72-0474, 11 August 1972.

Reagan, J. B., and T. M. Watt, "Simultaneous Satellite and Radar Studies of the D Region Ionosphere during the Intense Solar Particle Events of August 1972," *J. Geophys. Res.*, Vol. 81, 1 September 1976, p. 4579.

Reagan, J. B., et al., *Annual Technical Report for the Disturbed Media Satellite Program*, Lockheed Missiles and Space Company, LMSC-D-633113, December 1978.

Ulwick, J. C., "Comparison of Black Brant Rocket Measurements of Charged Particle Densities during Solar Particle Events," Chap. 26 in J. C. Ulwick (ed.), *Proceedings of COSPAR Symposium on Solar Particle Event of November 1969*, Air Force Cambridge Research Laboratories, AFCRL-72-0474, 11 August 1972, pp. 395-410.

Westerlund, S., F. Reder, and C. Åbom, "Effects of Polar Cap Absorption Events on VLF Transmissions," *Planet. Space Sci.*, Vol. 17, 1969, p. 1329.

DEPARTMENT OF DEFENSE

Assistant to the Secretary of Defense
Atomic Energy
    ATTN: Executive Assistant

Command & Control Technical Center
    ATTN: C-650

Defense Advanced Rsch. Proj. Agency
    ATTN: TIO

Defense Communications Agency
    ATTN: Code 810, J. Barna
    ATTN: Code 101B
    ATTN: Code 480, F. Dieter

Defense Communications Engineer Center
    ATTN: Code R410, R. Craighill
    ATTN: Code R410, J. McLean
    ATTN: Code R820

Defense Nuclear Agency
    ATTN: RAAE
    ATTN: STNA
4 cy ATTN: TITL

Defense Technical Information Center
12 cy ATTN: DD

Field Command
Defense Nuclear Agency
    ATTN: FCPR

Field Command
Defense Nuclear Agency
Livermore Division
    ATTN: FCPRL

Interservice Nuclear Weapons School
    ATTN: TTV

Joint Chiefs of Staff
    ATTN: C3S, Evaluation Office

Joint Strat. Tgt. Planning Staff
    ATTN: JLTW-2

National Security Agency
    ATTN: R-52, J. Skillman

NATO School (SHAPE)
    ATTN: U.S. Documents Officer

Undersecretary of Def. for Rsch. & Engrg.
    ATTN: Strategic & Space Systems (OS)

WWMCCS System Engineering Org.
    ATTN: R. Crawford

DEPARTMENT OF THE ARMY

BMD Advanced Technology Center
Department of the Army
    ATTN: ATC-T, M. Capps

DEPARTMENT OF THE ARMY (Continued)

Harry Diamond Laboratories
Department of the Army
    ATTN: DELHD-I-TL, M. Weiner
    ATTN: DELHD-N-P, F. Wimenitz
2 cy ATTN: DELHD-N-P

U.S. Army Comm.-Elec. Engrg. Instal. Agency
    ATTN: CCC-EMEO-PED, G. Lane

U.S. Army Foreign Science & Tech. Ctr.
    ATTN: DRXST-SD

U.S. Army Satellite Comm. Agency
    ATTN: Document Control

U.S. Army TRADOC Systems Analysis Activity
    ATTN: ATAA-PL

DEPARTMENT OF THE NAVY

Naval Electronic Systems Command
    ATTN: Code 501A
    ATTN: PME 106-4, S. Kearney
    ATTN: PME 106-13, T. Griffin

Naval Intelligence Support Ctr.
    ATTN: NISC-50

Naval Ocean Systems Center
    ATTN: Code 532

Naval Research Laboratory
    ATTN: Code 4780, S. Ossakow
    ATTN: Code 4700, T. Coffey
    ATTN: Code 7500, B. Wald
    ATTN: Code 7550, J. Davis

Naval Surface Weapons Center
    ATTN: Code F31

Strategic Systems Project Office
Department of the Navy
    ATTN: NSP-2722, F. Wimberly
    ATTN: NSP-2141

DEPARTMENT OF THE AIR FORCE

Air Force Geophysics Laboratory
    ATTN: PHP, J. Aarons
    ATTN: OPR-1, J. Ulwick
    ATTN: PHI, J. Buchau
    ATTN: PHP, J. Mullen

Air Force Technical Applications Center
    ATTN: TN

Air Force Weapons Laboratory
Air Force Systems Command
    ATTN: DYC
    ATTN: SUL

Air Force Wright Aeronautical Laboratories
    ATTN: A. Johnson

DEPARTMENT OF THE AIR FORCE (continued)

Ballistic Missile Office
Air Force Systems Command
    ATTN: MNNL, D. Kennedy

Foreign Technology Division
Air Force Systems Command
    ATTN: NIIS Library

Headquarters Space Division
Air Force Systems Command
    ATTN: SKA, M. Clavin

Rome Air Development Center
Air Force Systems Command
    ATTN: TSLD

Strategic Air Command
Department of the Air Force
    ATTN: XPFS, B. Stephan
    ATTN: ADWATE, B. Bauer
    ATTN: NRI

DEPARTMENT OF ENERGY CONTRACTORS

EG&G, Inc.
Los Alamos Division
    ATTN: J. Colvin
    ATTN: D. Wright

Lawrence Livermore National Laboratory
    ATTN: Technical Information Dept.

Los Alamos National Scientific Laboratory
    ATTN: J. Wolcott
    ATTN: R. Jeffries
    ATTN: MS 664, J. Zinn

Sandia National Laboratories
    ATTN: ORG 1250, W. Brown
    ATTN: D. Dahlgren
    ATTN: ORG 4241, T. Wright

OTHER GOVERNMENT AGENCIES

Central Intelligence Agency
    ATTN: OSI/PSID

Institute for Telecommunications Sciences
    ATTN: W. Utlaut

DEPARTMENT OF DEFENSE CONTRACTORS

Aerospace Corp.
    ATTN: I. Garfunkel
    ATTN: N. Stockwell
    ATTN: R. Slaughter

University of Alaska
    ATTN: Technical Library

APTEK
    ATTN: T. Meagher

Berkeley Research Associates, Inc.
    ATTN: J. Workman

Boeing Co.
    ATTN: D. Clauson

DEPARTMENT OF DEFENSE CONTRACTORS (continued)

Charles Stark Draper Lab., Inc.
    ATTN:
    ATTN:

Computer Sciences Corp.
    ATTN:
    ATTN:

Cornell University
    ATTN:

Electrospace Systems, Inc.
    ATTN:

EOS Inc.
    ATTN: Man
    ATTN:

General Electric
    ATTN: F. Nesbert

General Electric Company-TEMPO
    ATTN: W. Knapp
    ATTN: DASIAC

General Research Corp.
    ATTN: J. Garbarino
    ATTN: J. Ise, Jr.

University of Illinois
    ATTN: K. Yeh

Institute for Defense Analyses
    ATTN: E. Bauer

International Tel. & Telegraph Corp.
    ATTN: Technical Library

JAYCOR
    ATTN: J. Goldman

Johns Hopkins University
    ATTN: T. Potemra

Linkabit Corp.
    ATTN: I. Jacobs

M.I.T. Lincoln Lab.
    ATTN: D. Towle

McDonnell Douglas Corp.
    ATTN: Technical Library Services

Mission Research Corp.
    ATTN: R. Hendrick
    ATTN: F. Fajen
    ATTN: R. Bigoni
    ATTN: D. Lappinello
    ATTN: R. Bogusch

Mitre Corp.
    ATTN: R. Starr

Mitre Corp.
    ATTN: J. Aberle
    ATTN: W. Foster
    ATTN: W. Hall

49